Journal of Fluids and Structures (2000) **14,** 359–373
doi:10.1006/jfls.1999.0277, available online at http://www.idealibrary.com on IDEAL®

AN ANALYSIS ON COAXIAL JET FLOWS USING DIFFERENT DECOMPOSITION TECHNIQUES

T. YILMAZ

Yildiz Technical University, Department of Naval Architecture
80750 Yildiz, Istanbul, Turkey

AND

A. KODAL

Istanbul Technical University, Department of Aeronautical Engineering
80626 Maslak, Istanbul, Turkey

(Received 6 October 1998, and in final form 14 October 1999)

In this study, the Fourier transform, wavelet transform and turbulence filter methods have been applied to coaxial jet flows for various downstream positions in the inner and outer mixing regions. The data were obtained from cross-wire measurements, so axial and radial velocity components were acquired. Attention is focused on the characteristics of these signals in the initial region of the jet-flow field. The effects of some basic mechanisms of the vorticity dynamics on the velocity time histories, and on different statistical and spectral quantities, are studied.

1. INTRODUCTION

The flow produced by coaxial jets is of great interest from the perspective of aeronautical and industrial applications. Much of the aeronautical interest is related to noise reduction achievable by coaxial jets in comparison to simple jets. The effect of noise reduction by addition of a surrounding coaxial stream to a single jet has been observed (Williams *et al.* 1969). It has been suggested that the aerodynamic noise generated by simple and coaxial jets is related to the dynamics of large-scale vortical structures forming from the instability of the shear layers (Hussain 1986; Roshko 1976). The prediction of the dynamics of these structures by external forcing is necessary in order to have a better mixing between streams. This could be useful in industrial applications; e.g., in the design of new industrial burners for efficient combustion and minimum pollution. Large vortical structures play a role mainly in the initial region, where the azimuthal disturbances, if not intentionally introduced, do not have sufficient time to grow and influence the dynamics of the jets. Ko & Kwan (1976) studied coaxial jets by using hot-wire anemometry. They carried out measurements at different mean-velocity ratios and observed the similarity of the mean-velocity and turbulent-intensity profiles within the two mixing regions inside the initial merging zone, and within the mixing region inside the fully merged zone. They also showed similarities between coaxial and single jets. Petagna *et al.* (1994) have investigated the turbulent near-field of a coaxial jet using the wavelet transform. They showed that shear layer structures growing in size in the downstream direction dominate the field, even if their continuously varying shape and lack of regularity in presentation prevent their clear identification from Fourier spectral analysis, at least in the first stages of their development. Conversely, the wavelet-based procedure reveals clearly that only a limited range of scales

0889–9746/00/040359 + 15 $35.00/0

contributes to the Reynolds stress. Remarkably, they found that, even in the initial region of the outer jet core, where the Reynolds stresses are very small and the cross-spectra show no sign of prevailing frequencies, the contribution of the scales to the Reynolds stresses will become dominant at the end of the core. Onorato *et al.* (1996) studied velocity signals obtained from direct numerical simulations of an axisymmetric coaxial jet configuration, with inner-to-outer diameter and velocity ratios $D_i/D_0 = 0{\cdot}71$ and $U_i/U_o = 1{\cdot}41$, respectively. In their study, they focused on the characteristics of these signals in the initial region of the flow field, and analyzed effects of the basic mechanism of velocity dynamics on the velocity time-histories and on different statistical and spectral quantities. In particular, they used a wavelet cross-correlation analysis to associate the roll-up, the passage and the pairing of vortical structures with average, spectral and instantaneous contributions to the Reynolds stresses.

In this study, firstly, the Fourier and wavelet analyses of coaxial jet flows are carried out. Then, the flow characteristics in the initial region of coaxial jet flows are investigated by using the turbulence filter method (Kodal 1993). The turbulence filter method is applied to the data in order to decompose the velocity fluctuations into organized and nonorganized parts. The results of the turbulence filter are discussed, in the time, Fourier and wavelet domains.

2. EXPERIMENT AND DATA

It is well known that shear layers rapidly become unstable, and roll-up in discrete vortices, which grow, merge, and finally become turbulent. This evolution has been widely studied in the past for axisymmetric single jets (Hussain & Zaman 1985), but less effort has been devoted to study the effect of presence of an annular jet on the near-field dynamics of vortical structures. Characterization of such a coaxial jet flow-field is quite complex, due to the high number of parameters involved in a given configuration.

A typical flow-field of a coaxial jet configuration can be seen in Figure 1 for the condition of higher outer jet velocity. The measurements considered in this study were carried out in a research for the characterization of coaxial jets, at the Department of Aeronautical

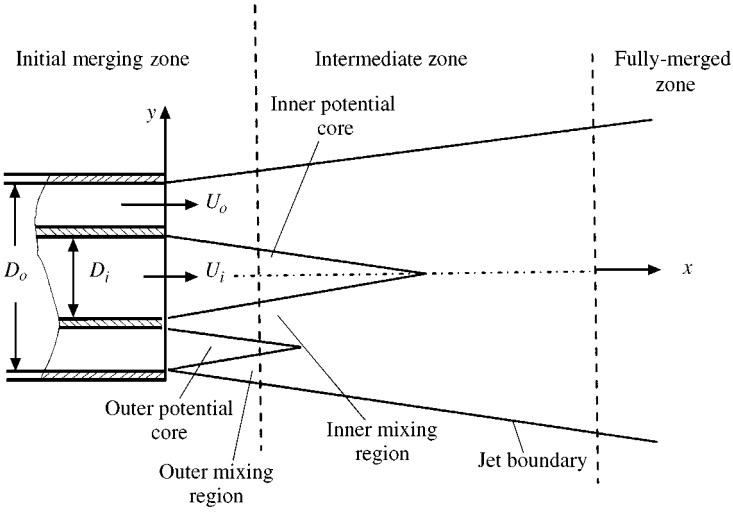

Figure 1. Flow field of a coaxial jet configuration.

Engineering, University of Pisa, Italy. The experimental facility and the instrumentation were described in detail by Buresti *et al.* (1994).

In axisymmetric flows, the boundary conditions have axial symmetry, mean values connected with the flow will be distributed with the same symmetry, and the flow is most conveniently described in cylindrical polar coordinates. The axis of symmetry is the x-direction, the radial coordinate is y, and the azimuthal coordinate is ϕ. The respective components of the mean velocity are U, V, W ($W = 0$ in axisymmetric flow), and the components of the instantaneous velocity fluctuations are u, v, w. In order to get a physical insight for the rolling-up and merging process of coaxial jets, it is necessary to consider only the azimuthal vorticity (Tso & Hussain 1989). Measuring the radial and axial velocities will allow the determination of the azimuthal vorticity. Therefore, many researchers have considered only the radial and axial components of the velocities in turbulent axisymmetric jet flows (Salvetti *et al.* 1996; Tso & Hussain 1989; Grinstein *et al.* 1995; Buresti *et al.* 1994). In addition, Townsend (1956) notes that the radial and azimuthal components of turbulence are nearly equal in a coaxial jet which infers that there is a similarity in the turbulence characteristics in these two directions.

In this study, the data were obtained by hot-wire anemometry using X-wire probes, therefore only the axial (u) and radial (v) velocity components have been considered. The signals from the probe were acquired at a sampling rate of 6000 Hz with a 12-bit A/D converter. In each measurement, 32 768 samples were acquired corresponding to signal duration of 5·46 s. The velocity signals were obtained at two radial distances ($y/D_i = 0{\cdot}4$ and 1) and four axial distances ($x/D_i = 1, 2, 3$ and 4). The thickness of the inner duct wall was negligibly small. In the measurements, the inner velocity, velocity ratio, inner duct diameter, diameter ratio and Reynolds number were $U_i = 1{\cdot}2$ m/s, $U_i/U_O = 0{\cdot}3$, $D_i = 77{\cdot}5$ mm, $D_i/D_O = 0{\cdot}5$ and $\mathrm{Re} = U_O D_O/\nu = 4{\cdot}2 \times 10^4$, respectively.

3. FOURIER ANALYSIS

The Fourier analysis has been widely used to characterize transitional flows in which interacting modes are dominant (Petagna *et al.* 1994; Onorato *et al.* 1996; Hussain & Zaman 1985; Davies *et al.* 1962; Anselmet *et al.* 1994). Alternatively, in order to describe the evolution of a fluctuating velocity component, u, and how its values at different times are related, one can also use auto-correlation function, $R_{uu}(\tau) = \overline{u(t)u(t+\tau)}$, which is related to the Fourier power spectrum. If the two component $u(t)$ and $v(t)$ of a velocity field are available, the Fourier cross-spectra can be defined as the Fourier transform of u times the complex conjugate of the Fourier transform of v. Using two velocity components, the cross-correlation function, $R_{uv}(\tau) = \overline{u(t)v(t+\tau)}$, can also be calculated.

The cross-spectrum $P_{uv}(\omega)$ is complex, so it can be expressed in terms of real and imaginary parts:

$$P_{uv}(\omega) = \mathrm{Co}P_{uv}(\omega) - \mathrm{i}\ \mathrm{Quad}P_{uv}(\omega). \tag{1}$$

The Fourier cospectrum $\mathrm{Co}P_{uv}(\omega)$ is the real part of the cross-spectrum and quad-spectrum $\mathrm{Quad}P_{uv}(\omega)$ is the imaginary part of the cross-spectrum. The phase angle $\theta_{uv}(\omega)$ between two signals is defined as

$$\theta_{uv}(\omega) = \tan^{-1}(\mathrm{Quad}P_{uv}(\omega)/\mathrm{Co}P_{uv}(\omega)). \tag{2}$$

These quantities are very useful because, besides giving information on the correlation between u and v in the Fourier and physical spaces, they are directly related to the Reynolds stress, $-\overline{\rho uv}$. For example, if $u(t)$ and $v(t)$ are in quadrature (i.e. their phase difference

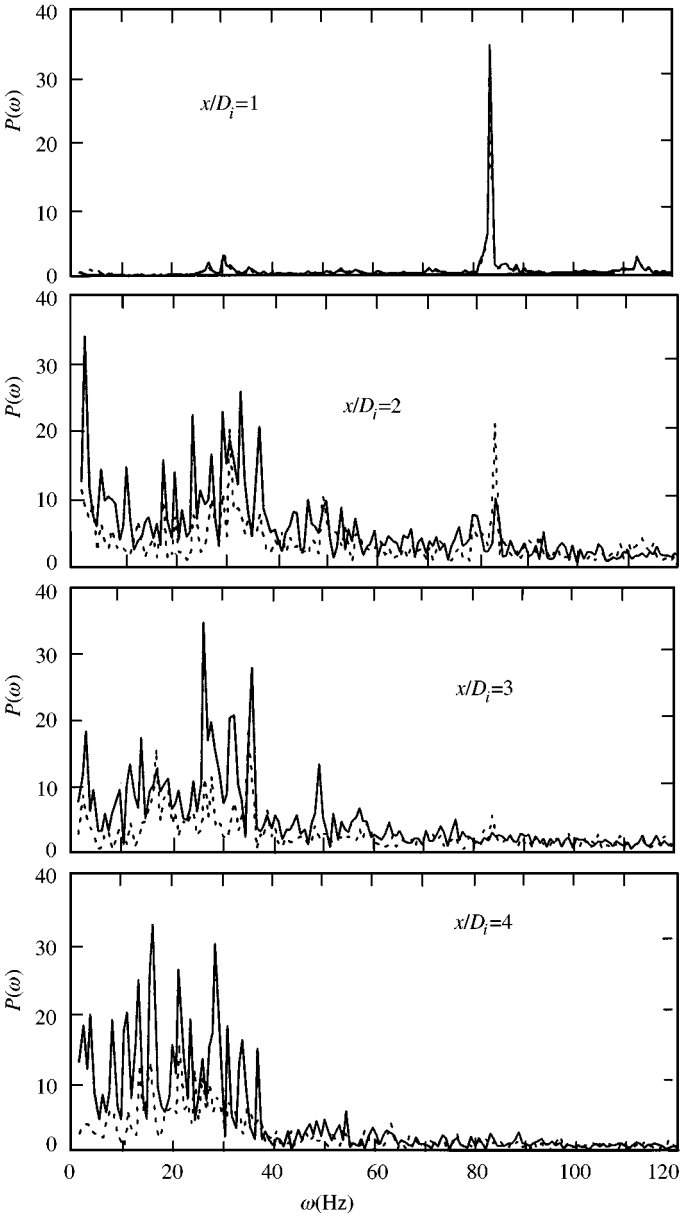

Figure 2. Power spectra of the u (solid line) and v (dotted line) velocities at four axial distances ($y/D_i = 0{\cdot}4$).

is 90°), then the cospectrum $\mathrm{Co}P_{uv}(\omega)$ and the contribution to Reynolds stress becomes zero. The nondimensional coherence function, C, is defined as

$$C = P_{uv}(\omega)/[P_u(\omega)P_v(\omega)]^{1/2} = C_r + \mathrm{i}C_i, \tag{3}$$

where C_r and C_i are the real imaginary parts of C, respectively (Roberts 1973).

The spectra of both axial (u) and radial (v) velocity components were considered at each measurement point. The analysis is based on the average of four spectra, obtained from portions of the hot-wire signals composed of 2^{13} samples, without overlapping. Figure 2 shows the linear power spectra of u and v velocity data for various downstream

distances at $y/D_i = 0{\cdot}4$. The linear power spectra give details on the prevailing frequencies. At the first point in the inner mixing region, ($y/D_i = 0{\cdot}4$, $x/D_i = 1$), a peak probably related to the passage of the large-scale structures at a dominant frequency is discernible. The u and v velocity power spectra are very similar. They have peaks at the frequencies of 32, 84 and 115 Hz. The peak at 84 Hz is the highest, so the most energetic motion can be expected at this frequency. At the second point ($y/D_i = 0{\cdot}4$, $x/D_i = 2$), the power spectra of u and v velocities show a few peaks at different frequencies. The u spectrum shows dominant peaks at frequencies of 2, 24, 30, 32 and 38 Hz, and the v spectrum shows two dominant peaks at 32 and 84 Hz. At this point, the motion at 84 Hz is less discernible in the axial direction but it is still effective in the radial direction. The motion at 32 Hz becomes more dominant in the axial and radial directions. At the third point ($y/D_i = 0{\cdot}4$, $x/D_i = 3$), the u spectrum shows dominant peaks 26, 32 and 36 Hz, and the v spectrum shows two dominant peaks at 17 and 32 Hz. At the last downstream point ($y/D_i = 0{\cdot}4$, $x/D_i = 4$), the dominant peaks can be seen at 17, 22 and 28 Hz for the u component, and at 22 Hz for the v component. As it can be seen clearly from Figure 2, the peaks tend to shift to lower frequencies in the downstream direction. This leads to the conclusion that the dimension of the vortical structures increases along the jet length. This result was also pointed out for coaxial jet by Petagna *et al.* (1994), who showed that shear-layer structures grow in size in the downstream direction.

The Fourier cospectra, quad-spectra and the coherence function at the first downstream station are presented in Figure 3 for the inner and outer mixing regions. The Fourier cospectrum of the first point shows a negative peak at a frequency of 84 Hz, which is the prevailing frequency in the u and v spectra at this location. The u and v velocities are correlated at this frequency. The quad-spectrum also shows a negative peak at 84 Hz, and this peak is approximately four times larger in magnitude than that of the cospectrum. The difference in magnitude of both spectra at 84 Hz corresponds to a large phase lag which can be determined as 80° by using equation (2). For the outer mixing region, the cospectra of the flow show opposite sign to those of the inner-mixing region. This is related to two vortex sheets of opposite sign, which originate from the inner and outer duct walls. It can be seen from the coherence plots that the real part of the coherence in the inner mixing region is found to be nearly zero over the whole frequency range considered. For the outer mixing region, the real part of the coherence is significantly nonzero. So the u and v velocity components are more correlated in the outer mixing region than in the inner mixing region.

It is not easy to determine the contribution of the mean flow to the Reynolds stress from the Fourier cross-spectral analysis. In the next section, the wavelet analysis will be presented; it gives a clearer representation than the Fourier analysis.

4. WAVELET ANALYSIS

4.1. Mathematical Formulation

The wavelet transform is a new processing tool that may help in extracting information from broad-band turbulent data allowing signal features to be identified *locally*, whereas the Fourier analysis requires regular repetition of events. A wavelet can be any real or complex-valued function, $\psi \in L^2$ (where L^2 denotes the Hilbert space of measure) that satisfies the wavelet admissibility condition

$$C_\psi = \int_{-\infty}^{\infty} |\hat{\psi}(\omega)|^2 |\omega|^{-1} \, \mathrm{d}\omega < \infty, \tag{4}$$

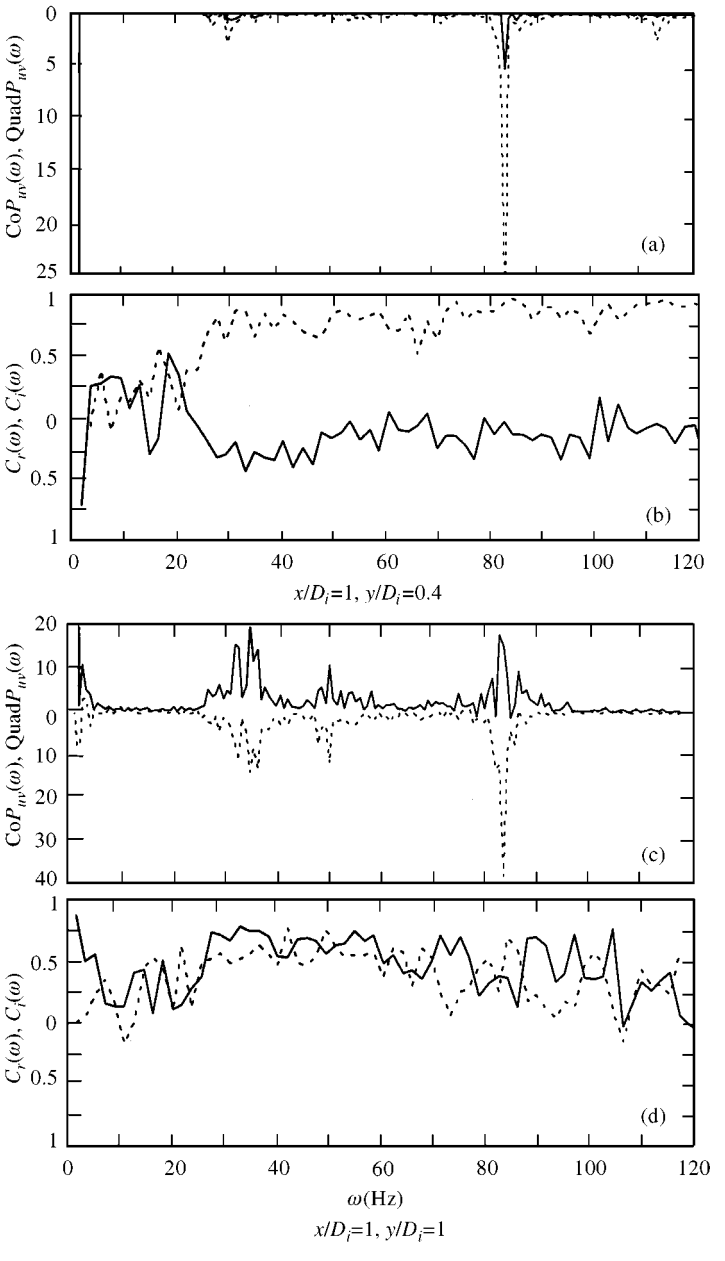

Figure 3. (a, c) Fourier co-spectra (solid lines), quad-spectra (dotted lines) and (b, d) coherence [$C_r(\omega)$ (solid lines), $C_i(\omega)$ (dotted lines)] at $x/D_i = 1$ and two radial distances.

where C_ψ is the admissibility constant, and $\hat{\psi}(\omega)$ is the Fourier transform of $\psi(t)$, i.e.,

$$\hat{\psi}(\omega) = \int_{-\infty}^{\infty} \psi(t)\, \mathrm{e}^{-\mathrm{i}\omega t}\, \mathrm{d}t. \tag{5}$$

Since $\psi(t) \in L^2$, condition (4) implies that $\psi(t)$ must have zero mean, and we have

$$\int_{-\infty}^{\infty} \psi(t)\, \mathrm{d}t = 0 \quad \text{or} \quad \hat{\psi}(\omega = 0) = 0. \tag{6}$$

The function $\psi(t)$ is called the mother wavelet and can be used to generate a wavelet family by continuous translation and dilation:

$$\psi_{a\tau} = p(a)\psi\left(\frac{t-\tau}{a}\right), \tag{7}$$

where $a \in \Re^+$ is the scale dilation parameter, $\tau \in \Re$ is the translation parameter corresponding to the position of the wavelet in the physical space, and $p(a)$ is a weighting function that can be chosen differently for different purposes. In the literature, the function $p(a)$ has been taken as $a^{-1/2}$, a^{-1} and a^0 (Farge 1992; Lewalle 1994; Arneodo *et al.* 1988). In the present work $p(a)$ was chosen as $a^{-1/2}$, so that the L^2—the norm of the wavelet—is independent of a and all wavelets have the same energy at each scale. The continuous wavelet transform of a function $f(t)$ is defined as the L^2 inner product between f and the wavelet $\psi_{a\tau}$,

$$W(a, \tau) = \int_{-\infty}^{\infty} f(t)\psi_{a\tau}^{*}\, \mathrm{d}t, \tag{8}$$

where $\psi_{a\tau}^{*}$ is the complex conjugate of $\psi_{a\tau}$. It should be pointed out that, for the continuous wavelet transform, the wavelets are not orthogonal and the transform contains redundant information. Nevertheless, owing to the admissibility condition (4), the signal $f(t)$ can be recovered from its wavelet coefficients,

$$f(t) = (1/C_\psi) \int_{-\infty}^{\infty} \int_{0}^{\infty} W(a, \tau)\psi_{a\tau}\, \mathrm{d}a\, \mathrm{d}\tau/a^2. \tag{9}$$

Furthermore, Parseval's equality holds,

$$\| f \|^2 = \int_{-\infty}^{\infty} |f(t)|^2\, \mathrm{d}t = (1/C_\psi) \int_{-\infty}^{\infty} \int_{0}^{\infty} |W(a, \tau)|^2\, \mathrm{d}a\, \mathrm{d}\tau/a^2. \tag{10}$$

Using the convolution thorem, it can be shown that the wavelet transform coefficients, equation (8), can also be calculated, for $p(a) = a^{-1/2}$, in the following way:

$$W(a, \tau) = (1/2\pi) \int_{-\infty}^{\infty} \hat{f}(\omega)[\hat{\psi}_a(\omega)]^*\, \mathrm{e}^{\mathrm{i}\omega\tau}\, \mathrm{d}\omega, \tag{11}$$

where $\hat{\psi}_a(\omega) = a^{1/2}\hat{\psi}(a\omega)$ is the Fourier transform of $a^{-1/2}\psi(t/a)$. Thus, at each scale a, $W(a, \tau)$ can be interpreted as a filtered version of $f(t)$, band-pass filtered by $\hat{\psi}_a(\omega)$. Equation (11) is very useful for the numerical computation of the wavelet coefficients.

In order to compare wavelet and Fourier results, it is useful to define the *scale number* $s = 1/a$, which plays the same role as the frequency in Fourier analysis. In terms of this new variable s, Parseval's equality changes to

$$\int_{-\infty}^{\infty} |f(t)|^2\, \mathrm{d}t = (1/C_\psi) \int_{-\infty}^{\infty} \int_{0}^{\infty} |W(s, \tau)|^2\, \mathrm{d}s\, \mathrm{d}\tau, \tag{12}$$

and the *wavelet power spectrum* can be defined as

$$P_W(s) = (1/C_\psi) \int_{-\infty}^{\infty} |W(s, \tau)|^2 \, \mathrm{d}\tau. \tag{13}$$

To relate the Fourier power spectrum $P_F(\omega) = (1/2\pi)|\hat{f}(\omega)|^2$ with the wavelet power spectrum, by using equations (11) and (13), the following relation is obtained:

$$P_W(s) = (1/C_\psi) \int_{-\infty}^{\infty} |\hat{\psi}_s(\omega)|^2 \, P_F(\omega) \, \mathrm{d}\omega, \tag{14}$$

where now $\hat{\psi}_s(\omega) = s^{-1/2} \hat{\psi}(\omega/s)$ is the Fourier transform of $\psi_s(\mathrm{t}) = s^{1/2}\psi(st)$. Thus, $P_W(s)$ is an average of the Fourier power spectrum $P_F(\omega)$, weighted by the power spectrum of the wavelet filter. Therefore, the wavelet analysis gives a smoother and clearer representation of the power spectrum than the Fourier analysis, and this feature can be used advantageously to determine the dominating frequencies in the spectra of the experimental turbulent velocity signals. However, it can be shown that for the wavelet spectra to actually reproduce the high wave number behavior of asymptotically decaying Fourier spectra, the analyzing wavelet must fulfill appropriate conditions, and, in particular, it must have enough vanishing moments.

The commonly used Morlet wavelet is a complex wavelet, which is used in this study; it is a sinusoidal wave multiplied by a Gaussian function,

$$\psi(t) = \mathrm{e}^{\mathrm{i}\omega_0 t} \, \mathrm{e}^{-t^2/2}. \tag{15}$$

In Fourier space, the Morlet wavelet is given by

$$\hat{\psi}(\omega) = (2\pi)^{-1/2} \, \mathrm{e}^{-(\omega - \omega_0)^2/2}. \tag{16}$$

The Morlet wavelet is only marginally admissible, because it has zero mean only if a small correction term is subtracted. In practice, if we take $\omega_0 = 6$, the correction term becomes unnecessary because it is of the same of a typical computer round-off error. For the Morlet wavelet, the relation between frequencies and scales is $\omega = \omega_0/(2\pi a)$.

The advantage of a complex wavelet, as we shall see in the cross-spectral analysis is that, the instantaneous phase of a signal or the difference of the phase between two signals can be defined. For this reason, all the applications of wavelet transform procedures to the analysis of velocity signals described in the present paper make use of the Morlet wavelet. Farge (1992) provides a good introduction to wavelet analysis as it applies to turbulence data. Mathematical details are covered in a number of recent books [e.g., Daubeches (1992)], while further information on recent applications may be found in Petagna *et al.* (1994), Lewalle (1994), and Hudgins *et al.* (1993).

4.2. Wavelet Spectral Analysis

The wavelet spectra and cross-spectra were obtained in order to find the dominant frequencies for the energy of fluctuations and the Reynolds stress production. In Figure 4, the wavelet energy scalogram [equation (8)] can be seen for the u velocity component for the first and third measurement points in the inner mixing region. This figure permits the identification of the intermittency of the events. As it can be seen from Figure 4(a), two dominant frequencies exist at 28 and 84 Hz for the first point, with the event at 28 Hz being more intermittent. In the Fourier analysis it is easy to obtain the frequency of the periodic motions, however the wavelet analysis gives information in time as well as in frequency. The u component wavelet scalogram is shown in Figure 4(b) for the position $y/D_i = 0{\cdot}4$, $x/D_i = 3$. From this figure, it is observed that there are some nearly periodic motions

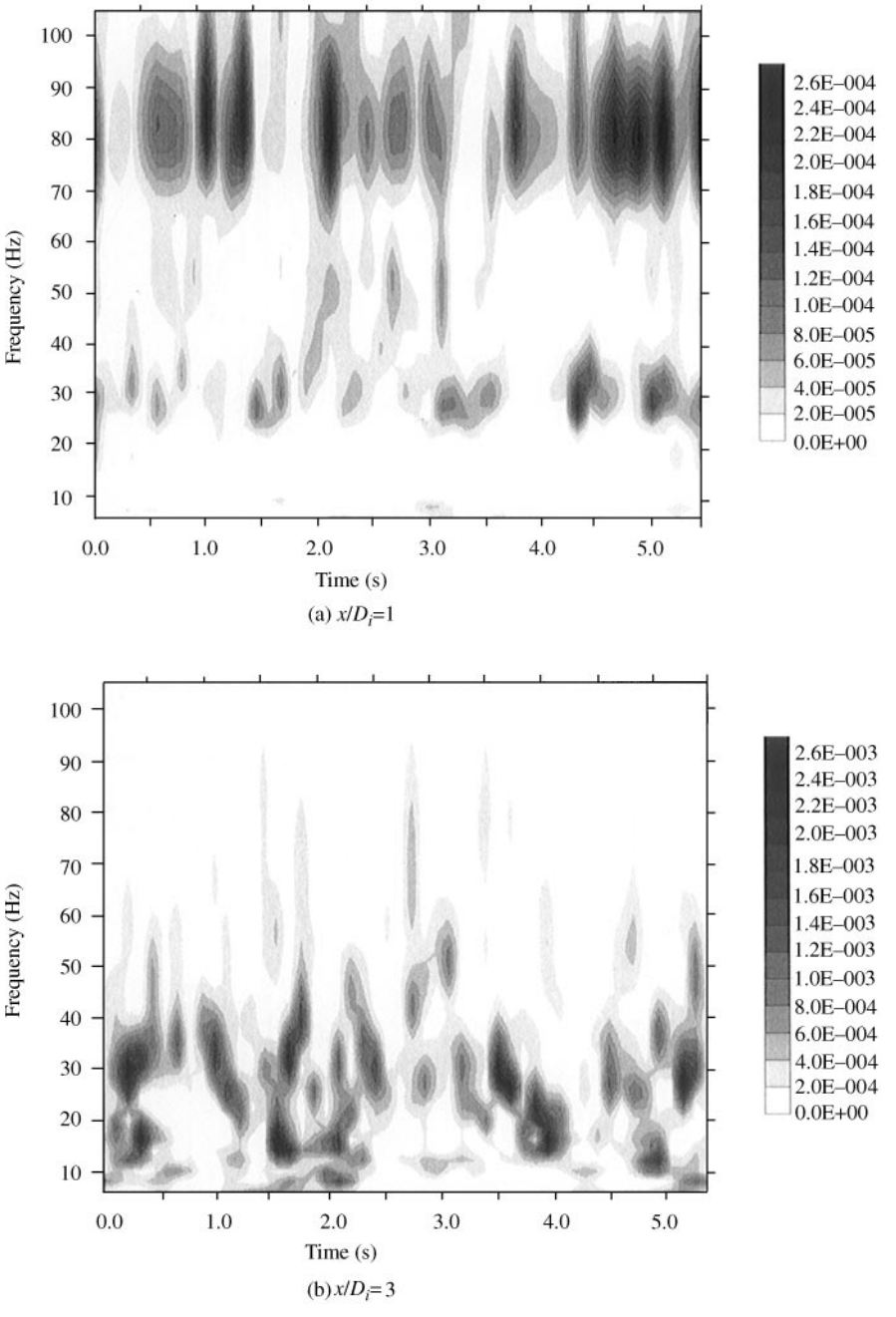

Figure 4. Wavelet scalogram of the u velocity component ($y/D_i = 0{\cdot}4$).

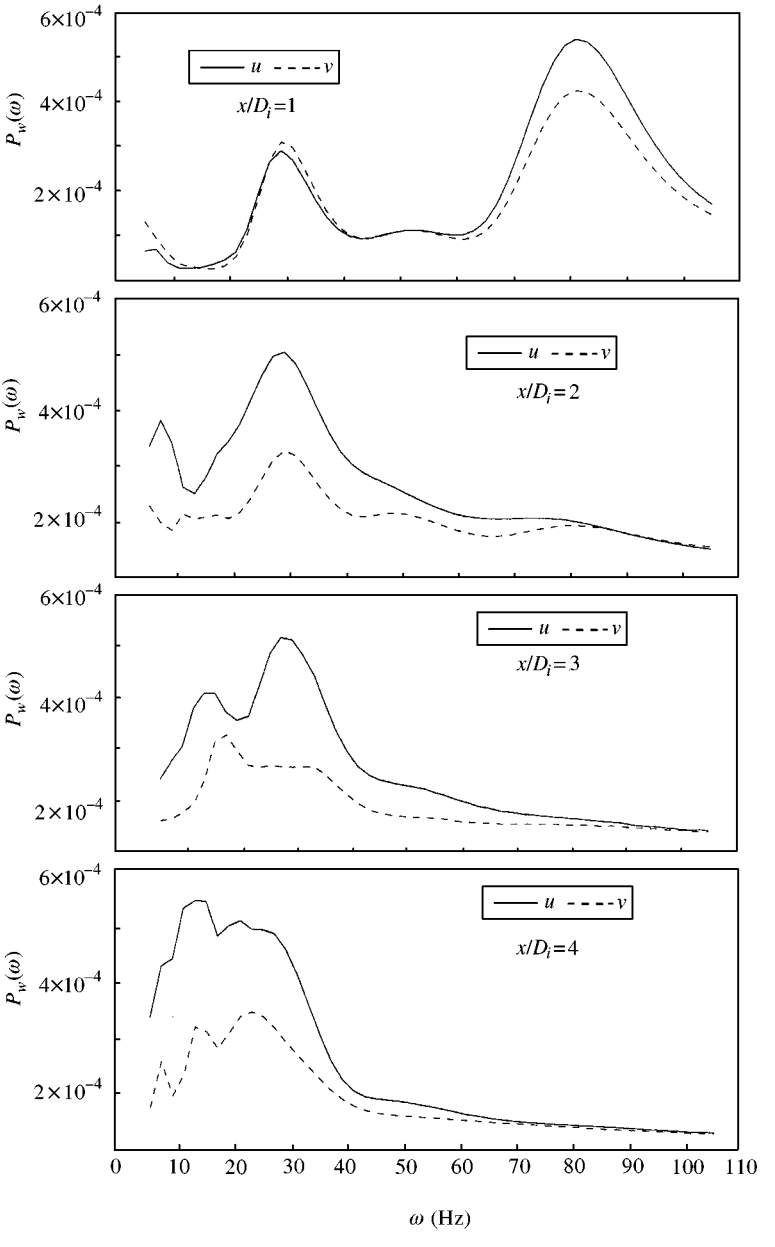

Figure 5. Wavelet power spectra of the total u and v velocities for four axial distances ($y/D_i = 0{\cdot}4$).

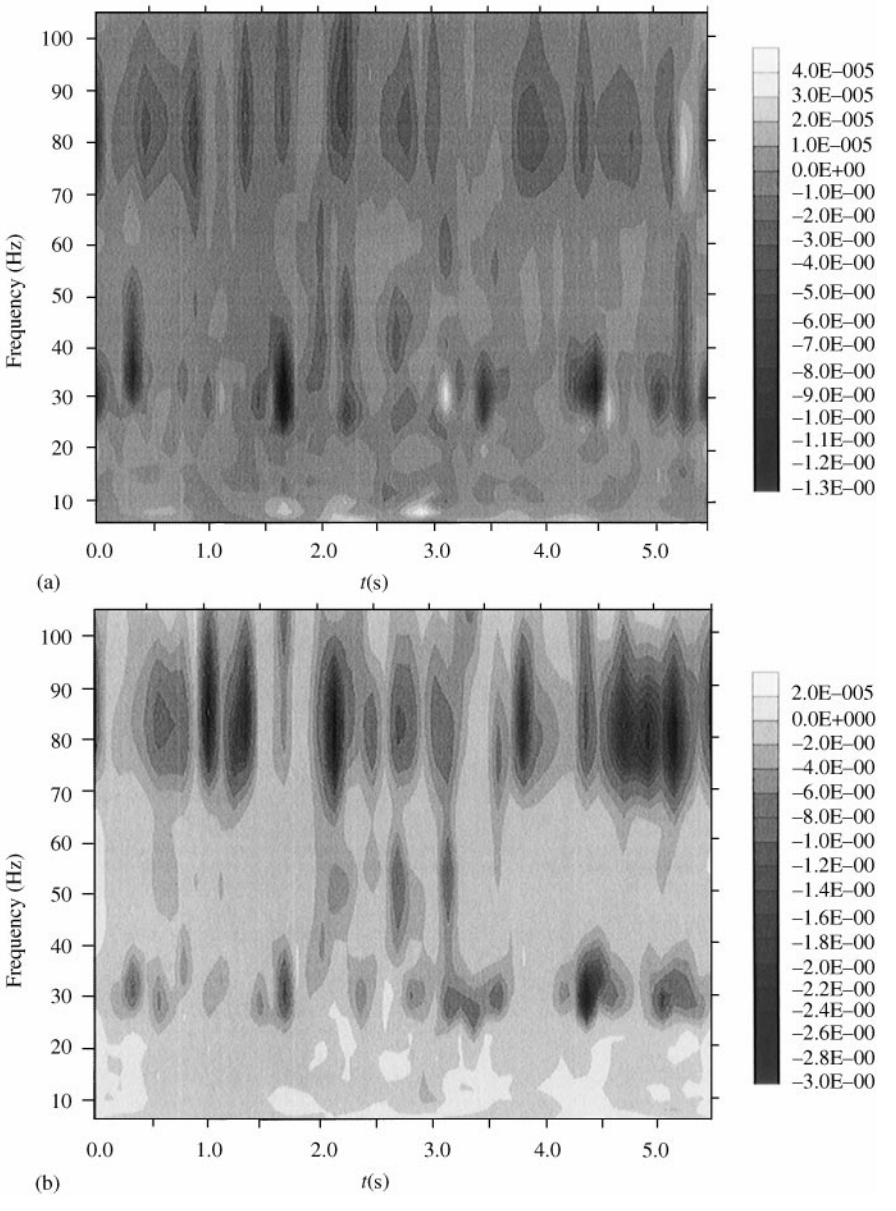

Figure 6. (a) Wavelet co-scalogram (b) wavelet quad-scalogram ($y/D_i = 0{\cdot}4$, $x/D_i = 1$).

concentrated around the frequencies of 14 and 28 Hz. The intermittency of these motions with time can also be observed.

The frequencies of these nearly periodic motions are clearer in Figure 5, which shows the wavelet power spectra of the u and v velocities in the inner mixing region. In Figure 5, the plot for the first measurement point ($x/D_i = 1$) shows two peaks at the frequencies of 28 and 84 Hz in both u and v wavelet power spectra. These peaks mean that there are nearly periodic motions at these frequencies. These motions are related to the vortex roll-up process. The frequency of 84 Hz corresponds to the vortex sheet rolling-up, and its subharmonic 28 Hz corresponds to the merging of the vortices. At the second downstream distance ($x/D_i = 2$), the peak at 28 Hz reaches a maximum value; this location is the first merging station of the vortices. The peak at 84 Hz at the first measurement point disappears. At the third point ($x/D_i = 3$), two different dominant frequency can be seen at 14 and 28 Hz. The peak at 14 Hz attains its maximum value at the last measurement point ($x/D_i = 4$), the second merging station.

4.3. Wavelet Cross-spectral Analysis

Let $W_u(a, \tau)$ and $W_v(a, \tau)$ be, respectively, the continuous wavelet transforms of two time signals $u(t)$ and $v(t)$. The wavelet cross-scalogram can be defined as follows:

$$W_{uv}(a, \tau) = W_u^*(a, \tau) W_v(a, \tau). \tag{17}$$

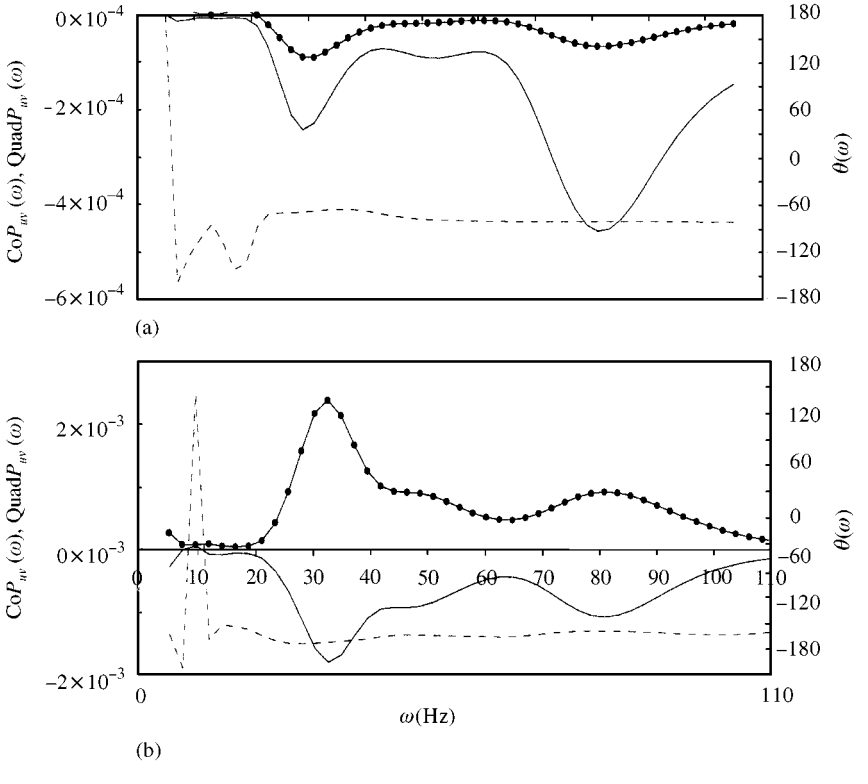

Figure 7. Wavelet co-spectra (solid line with circles), quad-spectra (solid line) and phase lag (dashed line) for $x/D_i = 1$ at two radial distances: (a) $y/D_i = 0{\cdot}4$; (b) $y/D_i = 1$.

If the analysis is carried out by means of a complex wavelet, as the Morlet wavelet used herein (Onorato *et al.* 1996), the cross-scalogram is also complex and can be written in terms of its real and imaginary parts, the coscalogram CoW_{uv} and the quad-scalogram Quad W_{uv}, respectively, i.e.,

$$W_{uv}(a, \tau) = \text{Co}\, W_{uv}(a, \tau) - \text{iQuad}\, W_{uv}(a, \tau). \tag{18}$$

The instantaneous angle of phase between $u(t)$ and $v(t)$ at the scale number a can also be defined as

$$\theta_{uv}(a, \tau) = \tan^{-1}(\text{Quad}\, W_{uv}(a, \tau)/\text{Co}\, W_{uv}(a, \tau)). \tag{19}$$

Since $u(t)$ and $v(t)$ are the two components of the velocity fluctuations in a turbulent flow, this formulation permits to detect time intervals and scales giving significant contributions to the Reynolds stress.

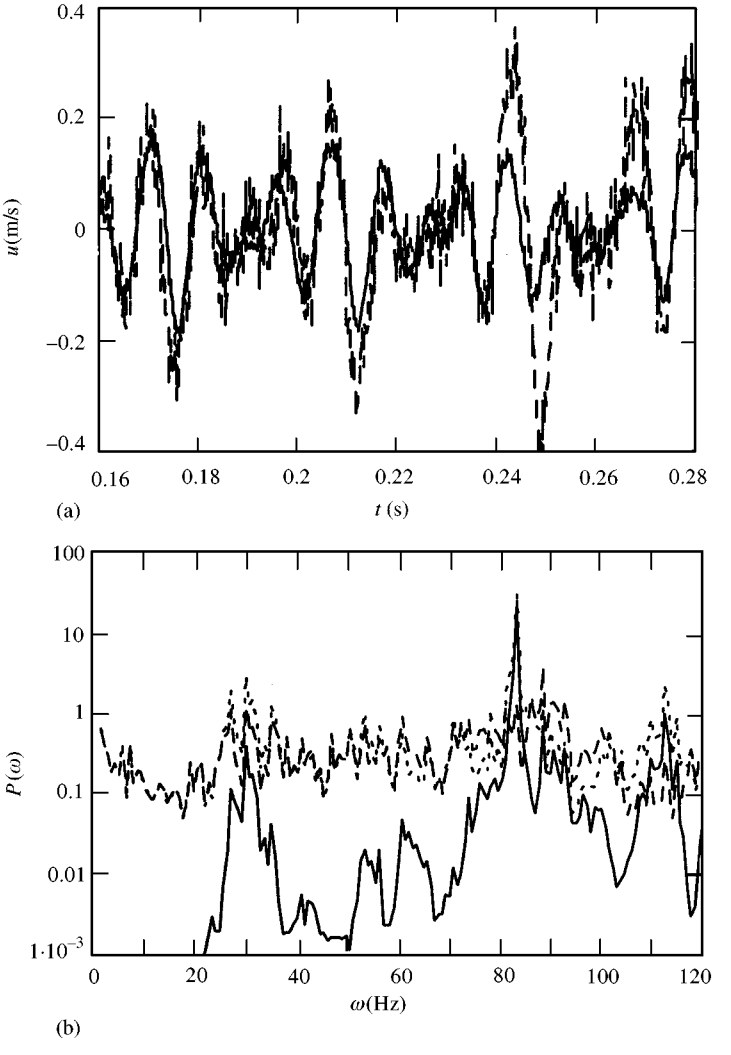

Figure 8. (a) Total u velocity data (dotted line) and filtered organized motion (solid line); (b) power spectra of the total data, filtered organized motion and filtered turbulent motion (dashed line); $y/D_i = 0{\cdot}4$, $x/D_i = 1$.

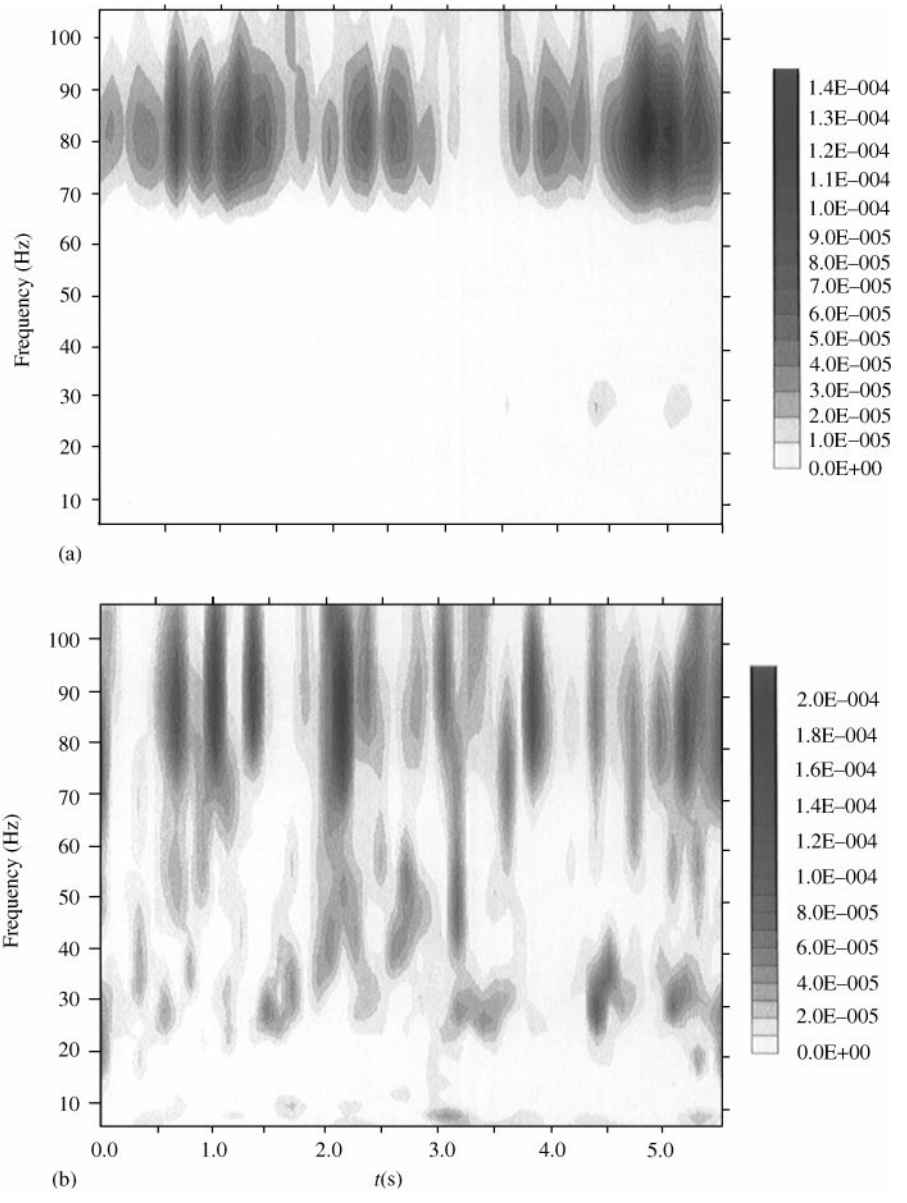

Figure 9. Wavelet scalograms for u velocity component: (a) filtered organized motion; (b) filtered turbulent motion; ($y/D_i = 0{\cdot}4$, $x/D_i = 1$).

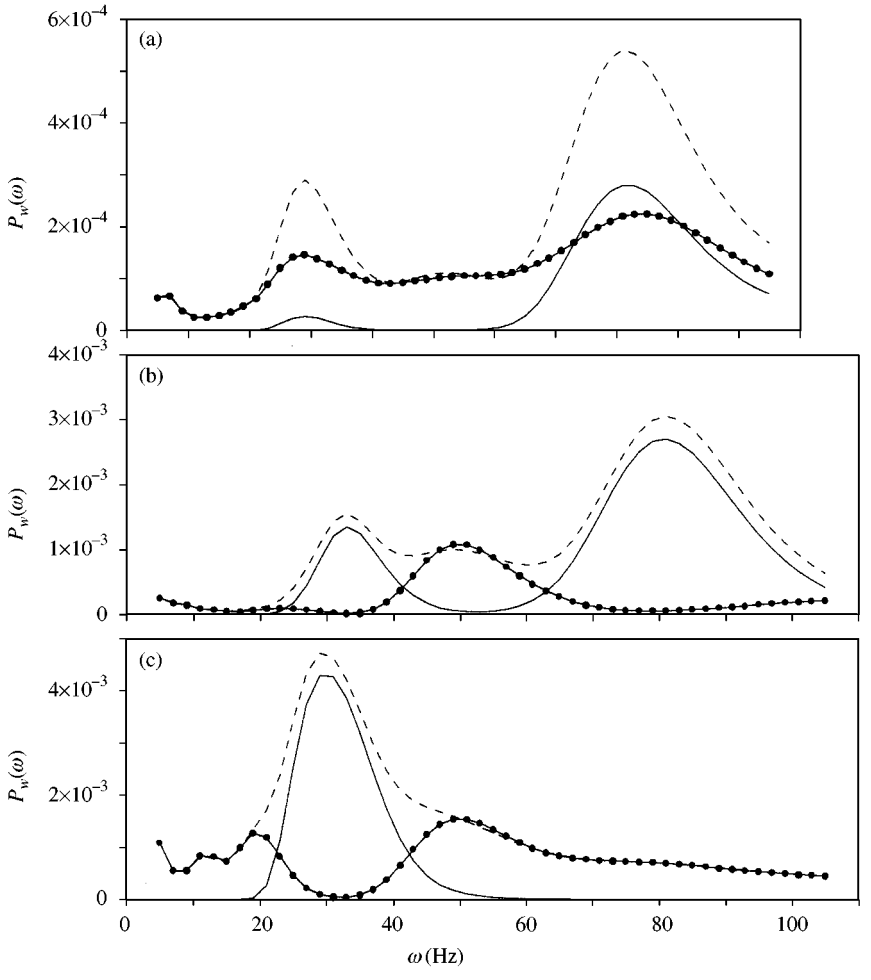

Figure 10. Wavelet power spectra of total velocity, filtered organized and filtered turbulent motions: (a) for the u velocity component ($x/D_i = 1$, $y/D_i = 0{\cdot}4$); (b) for the v velocity component ($x/D_i = 1$, $y/D_i = 1$); (c) for the v velocity component ($x/D_i = 2$, $y/D_i = 1$): - - -, total; ——, organized; –●–, turbulent.

The wavelet coscalogram and quad-scalogram are shown for the first measurement point in the inner mixing region in Figure 6. From the figure, we see concentrated spots around 28 and 84 Hz in both scalograms. The darkness of these spots indicates that these spots correspond to negative peaks. This can be seen clearly from Figure 7. In this figure, the wavelet cospectra, quad-spectra and phase lags of the u and v velocity components are shown for the inner and outer mixing regions at $x/D_i = 1$. For the inner mixing region, both spectrum curves show negative peaks at 84 Hz, however the peak of the quad-spectrum at this frequency is greater than that of the cospectrum. This implies that, the u and v components at this frequency have high phase lag (about 80°), and thus give a small contribution to $\overline{uv}$, i.e., to the Reynolds stress. It is interesting to point out that the cospectrum curve indicates a relatively larger negative peak at 28 Hz with respect to the peak at 84 Hz. Therefore, u and v velocities are more correlated and the phase difference between them is smaller at 28 Hz. The phase angle is about 60° at 28 Hz.

In Figure 7(b), the cospectra, quad-spectra and phase lags between u and v velocity components are presented for the outer mixing region. The cospectrum shows the opposite sign with the cospectra presented in the inner mixing region in Figure 7(a). This is related to two vortex sheets of opposite sign, which are originating from inner and outer duct walls as mentioned in the Fourier cross-spectra analysis. The highest correlation peak is seen at 32 Hz and a smaller peak at 84 Hz. It is interesting to point out that these peaks are at the same frequencies of the peaks of the inner mixing region. The quad-spectra have negative peaks at the same frequencies.

5. APPLICATION OF THE TURBULENCE FILTER

The turbulence filter is a relatively new decomposition technique. Brereton & Kodal (1992, 1994) applied the turbulence filter method to 1-D and 2-D turbulent flows and claimed that this method is more general than the phase average in its applicability and that it makes more efficient use of available data. In this section, we used the turbulence filter technique in order to decompose the near-field coaxial jet flow data into its organized and background turbulent components.

In Figure 8, the total u velocity data, filtered organized and turbulent motions in time and frequency domains can be seen for the first measurement point in the inner mixing region. The power spectrum of the filtered organized motion has a peak at the frequency of 84 Hz, associated with the vortex-sheet roll-up process. The wavelet transform can be used to analyze the filtered organized and turbulent motions in time–frequency plane. If a turbulent field is mainly some kind of noise, its energy density should be randomly distributed in both space and scale, without presenting any characteristic pattern in phase space (Farge 1992). The wavelet scalograms of the filtered organized and turbulent motions of the u velocity are shown in Figure 9 for the first measurement point in the inner mixing region. The wavelet map of the filtered organized motion shows dominant frequency at 84 Hz with an intermittent character. In the turbulence map, the energy density is randomly distributed in both time and frequency, as expected.

The wavelet power spectra of the total data, organized and turbulent motions are presented in Figure 10(a) for this point. The power spectrum of the filtered organized motion shows dominant frequencies at 28 and 84 Hz which are the roll-up and merging frequencies of the vortices. In Figure 10b, c, the wavelet power spectra of the filtered organized and turbulent motions of the v velocity are presented for the first two downstream distances in the outer mixing region. At the first point, the power spectrum of the filtered organized motion has two dominant peaks at 32 and 84 Hz. The peak at 84 Hz is higher than the one at 32 Hz, corresponding to relatively more energetic motion. The spectrum of the turbulent component has almost zero energy at these frequencies. At the second point, which iss the first merging location, the spectrum of the filtered organized motion shows a dominant peak at 32 Hz and the filtered turbulent component has almost zero energy at this frequency.

6. CONCLUSIONS

The flow-field structures of the coaxial jet flows were analyzed with different decomposition techniques. Firstly, the Fourier analysis of the initial region of the coaxial jet flow has been carried out. The roll-up and merging frequencies of the vortices are presented in the Fourier spectral and cross-spectral analysis. The analysis using the wavelet transform has allowed examining the intermittency of the flow and showed clearer representation. The rolling-up and merging frequencies are seen in the wavelet presentation better than the Fourier

analysis. Finally, the turbulence filter method is used to decompose the flow into organized and nonorganized components. The wavelet maps of the filtered organized and turbulent motions have been demonstrated. The wavelet map of the filtered organized motion showed a dominant frequency with an intermittent behavior, and the wavelet map of the filtered turbulence showed randomly distributed character in time and frequency domain.

ACKNOWLEDGEMENT

This study was supported in scope of the NATO Science Fellowship Program by The Scientific and Technical Research Council of Turkey (TUBITAK). The authors wish to thank Prof. G. Buresti and Prof. G. Lombardi for their valuable help.

References

Adrian, R. J. 1975 On the role of conditional averages in turbulence theory. In *Proceedings of the* 4*th Biennial Symposium on Turbulence in Liquids* (eds J. L. Zakin & G. K. Patterson), pp. 322–330. Princeton: Science Press.

Anselmet, F., Djeridi, H. & Fulachier, L. 1994 Joint statistics of a passive scalar and its dissipation in turbulent flows. *Journal of Fluid Mechanics* **280,** 173–197.

Arneodo, A., Gresseau, G. & Holschneider, M. 1988 Wavelet transform of multifractals. *Physics Review Letters* **61,** 2281–2284.

Brereton, G. J. & Kodal, A. 1992 Frequency-domain filtering technique for triple decomposition of unsteady turbulent flow. *ASME Journal of Fluids Engineering* **114,** 45–51.

Brereton, G. J. & Kodal, A. 1994 An adaptive turbulence filter for decomposition of organized turbulent flows. *Physics of Fluids* **6,** 1775–1786.

Buresti, G., Talamelli, A. & Petagna, P. 1994 Experimental characterization of the velocity field of a coaxial jet configuration. *Experimental Thermal and Fluid Science* **9,** 135–146.

Daubeches, I. 1992 *Ten Lectures on Wavelets.* Philadelphia, PA: SIAM.

Davies, P. O., Fisher, M. J. & Barratt, M. J. 1962 The characteristics of turbulence in the mixing region of a round jet. *Journal of Fluid Mechanics* **15,** 337–367.

Farge, M. 1992 Wavelet transforms and their application to turbulence. *Annual Review of Fluid Mechanics* **24,** 395–457.

Grinstein, F. F., Glauser, M. N. & George, W. K. 1995 Vorticity in jets. In *Fluid Vortices* (ed. S. I. Green), pp. 65–94. Dordrecht: Kluwer Academic Publishers.

Ho, C. M. & Huang, L. S. 1982 Subharmonics and vortex merging in mixing layers. *Journal of Fluid Mechanics* **119,** 443–473.

Hudgins, L., Friehe, C. A. & Mayer, M. E. 1993 Wavelet transforms and atmospheric turbulence. *Physics Review Letters* **71,** 3279–3282.

Hussain, A. K. M. F. 1986 Coherent structures and turbulence. *Journal of Fluid Mechanics* **173,** 303–356.

Hussain, F. & Zaman, K. 1985 An experiment study of organized motions in the turbulent plane mixing layer. *Journal of Fluid Mechanics* **159,** 85–104.

Ko, N. W. M. & Kwan, A. S. H. 1976 The initial region of subsonic coaxial jets. *Journal of Fluid Mechanics* **73,** 305–332.

Kodal, A. 1993 A new orthogonal decomposition method for turbulent flows. Ph.D. Thesis, The University of Michigan.

Lewalle, J. 1994 Wavelet analysis of experimental data: some methods and the underlying physics. *AIAA Journal* **94,** 2281–2288.

Onorato, M., Salvetti, M. V., Buresti, G. & Petagna, P. 1996 Analysis of DNS velocity signals in a coaxial jet configuration. *Aerospaziale*, *Universita Degli Studi di Pisa. Dipertimento di Ingegneria.* 96–10.

Petagna, P., Lewalle, J. & Buresti, G. 1994 Wavelet analysis of the turbulent near-field of a coaxial jet. In *Advances in Turbulence V*, *Proceedings of the Fifth European Turbulence Conference*, Siena, Italy, (ed. Roberto Benzi), pp. 413–417. Dordrecht: Kluwer Academic Publishers.

Roberts, J. B. 1973 Coherence measurements in an axisymmetric wake. *AIAA Journal* **11,** 1569–1571.

Roshko, A. 1976 Structure of turbulent shear flows: A new look. *AIAA Journal* **14,** 1349–1355.

Salvetti, M. V., Orlandi, P. & Verzicco, R. 1996 Numerical simulations of transitional axisymmetric coaxial jets. *AIAA Journal* **34,** 736–743.

Townsend, A. A. 1956 *The Structure of Turbulent Shear Flow* Cambridge: Cambridge University Press.

Tso, J. & Hussain, F. 1989 Organized motions in a fully developed turbulent axisymmetric jet. *Journal of Fluid Mechanics* **203,** 425–448.

Williams, T. J., Ali, M. R. M. H. & Anderson, J. S. 1969 Noise and flow characteristic of coaxial jets. *I. Mech. E. Journal of Mechanical Engineering Science* **2,** 133–143.